Colloids and Surfaces B: Biointerfaces 141 (2016) 565–575

Contents lists available at ScienceDirect

Colloids and Surfaces B: Biointerfaces

journal homepage: www.elsevier.com/locate/colsurfb

Self-organization of gliadin in aqueous media under physiological digestive pHs

María G. Herrera[a], Tania V. Veuthey[a], Verónica I. Dodero[a,b,*]

[a] Departamento de Química-INQUISUR, Universidad Nacional del Su- CONICET, Av. Alem 1253, Bahía Blanca, Argentina
[b] Universität Bielefeld, Fakultät für Chemie, Organische Chemie, Universitätsstr. 25, 33615 Bielefeld, Germany

ARTICLE INFO

Article history:
Received 9 October 2015
Received in revised form 2 February 2016
Accepted 8 February 2016
Available online 10 February 2016

Keywords:
Gliadin nanostructures
Nile red binding
Biophysics
Colloids
Electron microscopy
Gliadin related disorders

ABSTRACT

Here we showed that gliadin, a complex protein system related to celiac disease and other human diseases, is spontaneously self-organized in a very dilute solution at pH 3.0 and 7.0 in water under low ionic strength (10 mM NaCl). The spontaneous self-organization at pH 3.0 increases the apparent solubility due to the formation of finite sized aggregates, such as those formed in the micellization of amphiphilic molecules. Switching the pH from 3.0 to 7.0 lead to a phase separation, however part of the nano-particles are stable remaining disperse in water after centrifugation. Also, beside the pH change led to changes in protein composition and concentration, we determined that the secondary structure of both system is the same. Moreover, Tyrs are slightly more buried and Trps are slightly more exposed to water at pH 7.0 than those at pH 3.0. Electron microscopy techniques showed that both gliadin systems are composed of nanostructures and in the case of pH 7.0 amorphous microaggregates were found, too. Only nanostructures at pH 3.0 showed a micromolar binding affinity to Nile red probe, suggesting the presence of accessible hydrophobic patches which are not more accessible at pH 7.0. All our results suggest that gliadin is able to self-organized at pH 3.0 forming protein micelles type nanostructures ($\zeta = +13$, 42 ± 1.55 mV), meanwhile at 7.0 the decrease of superficial charge to ζ of +4, 78 ± 0.48 mV led to the formation of stable colloidal nanoparticles, unable to interact with Nile red probe. Our findings may open new perspectives for the understanding of gliadin ability to avoid proteolysis, to reach and cross the intestinal lumen and to trigger different immunological disorders.

1. Introduction

Gliadin is a complex protein mixture present in wheat, rye and barley which is not fully degraded by humans [1]. It is composed of different fractions which can be classified into four groups: the ω gliadin (72 and 80 KDa) that cannot be further reduced; and α, β (33, 34, 35, 41, 43 and 47 KDa) and γ-gliadin (49 and 57 KDa) which are reduced to polypeptides of slightly lower electrophoretic mobility than their precursors [2]. Early reports have shown that gliadin, as the whole mixture, is soluble in alcohols but the solubility in water is low [3]. Thus much effort has been done to increase gliadin water solubility in order to isolate and characterize different gliadin isoforms [3–5]. In some cases, the formation of self-assembled complexes, like nanofibrils of α-gliadin in water at pH 5.0 in 0.01 M acetic acid and 0.005 of ionic strength has been reported [6]. Indeed, its low solubility in water has been used to synthetize gliadin nanoparticles and nanocapsules for drug delivery, mainly from gliadin extracts in ethanol/water (70/30) obtained by desolvatation methods [7–9]. Recently, α, β and γ-gliadin were extracted from wheat dough in water by NaCl gradients [10]. On the other hand, it is known that gliadins and some of its proteolytic resistant peptides are responsible for immunological diseases [11]. The most known gliadin related disease is celiac disease which is a complex immunological disorder with a prevalence of 1% among the healthy population [12,13]. Recently, a new pathology named gluten sensitivity has been described, showing higher prevalence than celiac disease, an estimated 7% of the total population [13,14]. Up to now, the only treatment for both pathologies is a gliadin-free long-life diet [15].

Despite intensive studies, the primary mechanism by which gliadin and its proteolytical resistant fragments cause immunological imbalance and disease still remains to be elucidated [12,15]. Recently, the self-assembly capability of gliadin immunogenic peptide known as 33-mer was reported, under physiological rel-

* Corresponding author at: Departamento de Química–INQUISUR, Universidad Nacional del Sur–CONICET. Av. Alem 1253, 8000 Bahía Blanca, Argentina.
E-mail addresses: veronica.dodero@uns.edu.ar, veronica.dodero@uni-bielefeld.de (V.I. Dodero).

http://dx.doi.org/10.1016/j.colsurfb.2016.02.019
0927-7765/

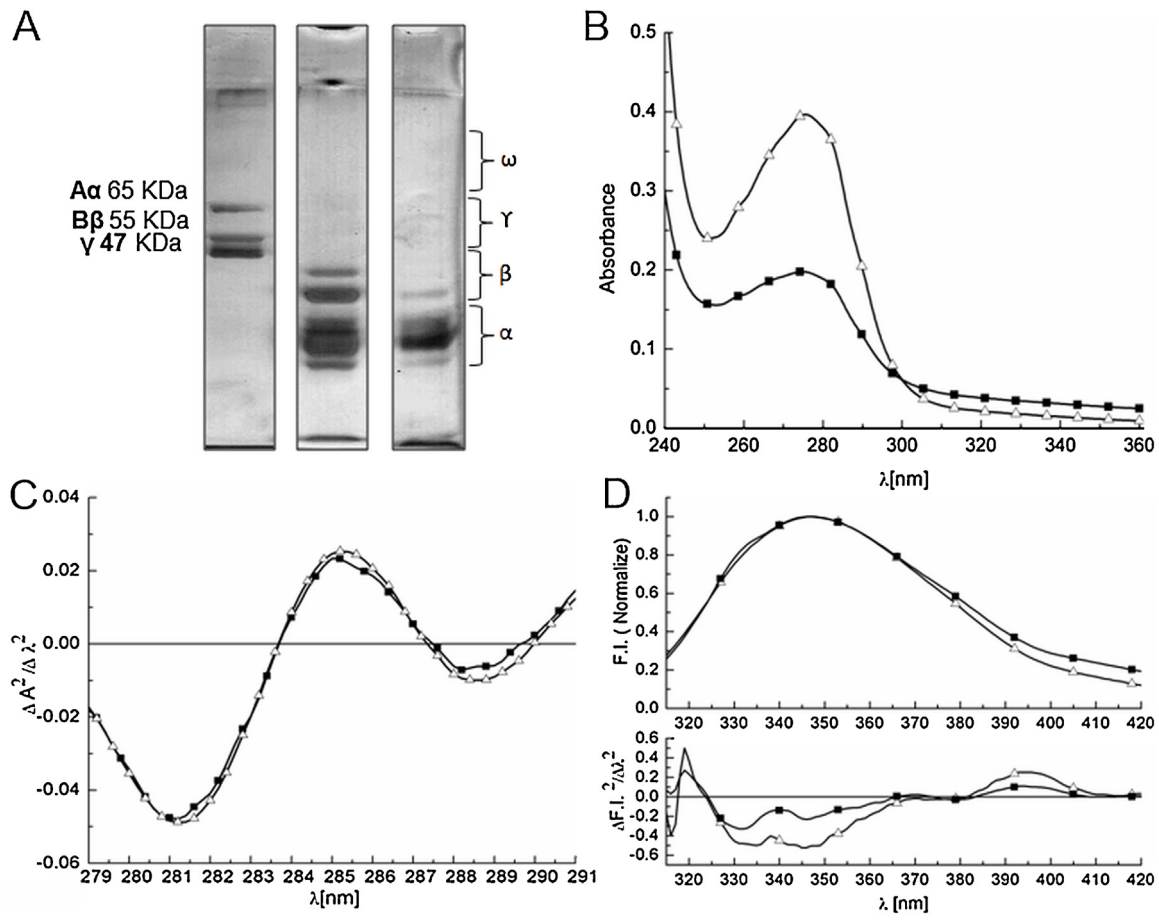

Fig. 1. (A) SDS-PAGE of Gliadin system at pH 3.0 (lane 2) and after pH 7.0 was reached (lane 3). Fibrinogen was used as molecular weight marker (lane 1); B) UV–vis Spectra of gliadin systems at pH 3.0 (△) and after pH 7.0 was reached (■); (C) Second derivate of UV–vis spectra of gliadin systems at pH 3.0 (△) and 7.0 (■) showing the region between 280 and 292 nm (Tyrosine and tryptophan absorption sensible range). (D) Normalized fluorescence emission spectra of gliadin systems and the corresponding second derivative spectra at pH 3.0 (△) and 7.0 (■). Measurements were performed exciting samples at 295 nm at 25 °C.

evant conditions [16]. A conformational equilibrium toward a beta-parallel structure was reported in the case of 33-mer [17]. Importantly, the beta parallel sheet is a structural signature for other protein related diseases like Alzheimer' s disease and Parkinson' s disease [18]. Considering the direct association of gliadin protein and some immunological disorders, we envisaged the importance to understand gliadin self-organization capability in water under gastrointestinal (GI) environment conditions. Recently, the mammalian GI tract parameters which modulate the absorption of food relevant nanomaterials have been reported. It has been shown that pH is one of the most important parameters, varying from pH 2.0 to pH 8.0 [19]. Initially, saliva has a neutral value of 7.0. Although the pH in the stomach can be as low as 1, food induces a buffered effect, showing values in the range of 2.0–6.0. Finally, in the small and large intestine lumen the pH ranges from 5.0 to 8.0. In addition, it is well described that gliadin is not fully degraded in the stomach nor in the duodenum environment and that all the immunological experiments has been done in water with the soluble fraction of gliadin at pH 7.0 [1,12,20,21]. Here, we evaluated gliadin water soluble fraction at relevant physiological pH such as 3.0 and 7.0 at 10 mM NaCl. The physico-chemical evaluation was done by spectroscopic experiments such as UV–vis, Fluorescence, and circular dichroism in combination with ζ potential measurements and morphological characterization by SEM and TEM. Finally, Nile red experiments revealed that the nature of both gliadin self-organized systems is different. Altogether, our findings showed that gliadin is spontaneously self-organized into micelles type aggregates at pH 3.0, meanwhile although at pH 7.0 an initial phase separation occurrs, gliadin colloidal nanoparticles are stabilized after centrifugation, probably by H-bonds between gliadin's exposed amino acids and water.

2. Materials and methods

2.1. Sample preparation

Wheat gliadin was purchased from Sigma-Aldrich. A solution of gliadin 1.0 mg/ml was prepared in 0.001 M HCl, NaCl 10 mM, pH 3.0. MilliQ water filtered through Nylon 0.2 μm membrane was used to prepare all the solutions. Gliadin solution was homogenized at room temperature, stabilized by 12 h at 10 °C and centrifuged at 1288 g. Finally, supernatant was separated in two aliquots. One of them was brought to pH 7.0 with 0.1 M NaOH (2 μL) when needed adjustment has been done by 0.001 M HCl. After pH 7.0 was reached, phase separation occurred. Both gliadin systems, at pH 3.0 and 7.0 were centrifuged at 21130*g* for 15 min and supernatants were collected. By Bradford assay, the soluble concentration of gliadin at pH 3.0 and 7.0 was calculated as 0168 mg/ml and 0065 mg/ml, respectively. All experiments were performed with visible clear solutions at 25 °C. Both colloidal suspension were stable in our measurement time scales (up to 24 h). The above mentioned protocol was established to obtain reproducibility between protein batches.

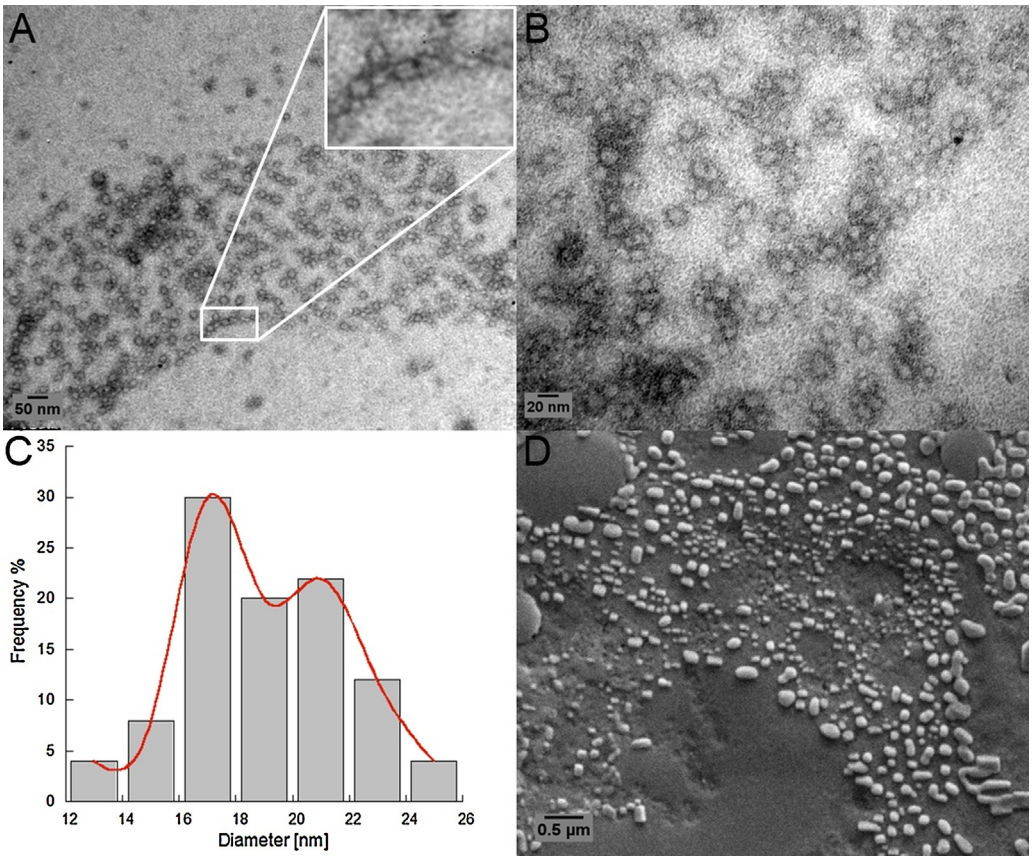

Fig. 2. EM microphotographs of gliadin system at pH 3.0, NaCl 10 mM. (A) TEM image of the particles deposited on a Formvar grid and a zoom the nanostructures observed. (B) Zoom of a region of image A, showing the local arrange of the particles. (C) Diameter Distribution of the particles observed in image A. (D) SEM Images showing the fractal arrange of gliadin nanostructures on a glass surface.

2.2. Characterization of gliadin composition by SDS-PAGE

Soluble gliadin fractions were identified by SDS-PAGE: 15 μg of gliadin solutions pH 3.0 and 7.0 were prepared in Laemmli buffer (1.5 M Tris pH 6.8, 20% SDS, 10% 2-ME, 20% glycerol, 2% Bromophenol Blue) and electrophoresed on 8% gel at 150 V for 1.5 h. Fibrinogen was used as molecular weight marker showing 3 bands: α of 65 KDa, β of 55 KDa and γ of 47 KDa [22]. At the end of the experiment, protein bands were visualized by a standard silver staining.

2.3. UV–vis spectroscopy

UV–vis spectra of gliadin solutions were acquired at pH 3.0 (0.168 mg/ml) and 7.0 (0.065 mg/ml). The spectroscopic study was performed by a spectral scanning between 240 and 400 nm at 25 °C using a V-630 BIO JASCO spectrophotometer coupled to a Peltier system. The second derivative spectrum of each solution was obtained using OriginLab software. For each spectrum a smooth of 30 points was employed using Savitzky-Golay algorithm based on a second order function.

The aggregation index (A.I. [%]) was determined by Eq. (1) [23], (Eq. (1)). According to this index the following scale was utilized: (a) between 0 and 2: solution; (b) between 2 and 5: some aggregates formation; (c) >5: high aggregation.

$$I.A.\,[\%] = \left(\frac{100 \times A_{350}}{A_{280} - A_{350}}\right). \quad (1)$$

Determination of tyrosine: tryptophan (Tyr: Trp) ratio was performed according to the method of Bencze and Schmid [24]. To this aim, working gliadin solutions at pH 3.0 and 7.0 were treated with NaOH to reach a final concentration of 0.1 M NaOH, pH 12.0. UV–vis spectra were acquired and the ratio between both amino acids was determined by extrapolation analysis with theoretical data presented by Bencze and Schmid [24] (see Supplementary information, SI)

2.4. Zeta potential

The zeta potential (ζ) of gliadin systems at both conditions was measured by the Zetasizer (Nano-ZS) from Malvern Instruments and its software, Dispersion Technology Software (DTS).

2.5. Steady state tryptophan intrinsic fluorescence spectroscopy

Solutions of gliadin at pH 3.0 (0.168 mg/ml) and 7.0 (0.065 mg/ml) were excited at 295 nm and emission signal was collected between 300 and 450 nm using an excitation and emission slits of 5 nm. Spectra were acquired at 25 °C using a Shimadzu RF spectrofluorophotometer. The accurate λ_{max} emission was determined by second derivative method.

2.6. Electron microscopy

2.6.1. Scanning electron microscopy (SEM)

A gliadin aliquot (20 μL) was deposited on uncoated coverslips and let dry in a Petri-dish. Resulting specimens were metalized with Au(0) using Sputter coater Pelco 91000 and observed via a JSM-35CF equipped with secondary electron detector (EVO 40).

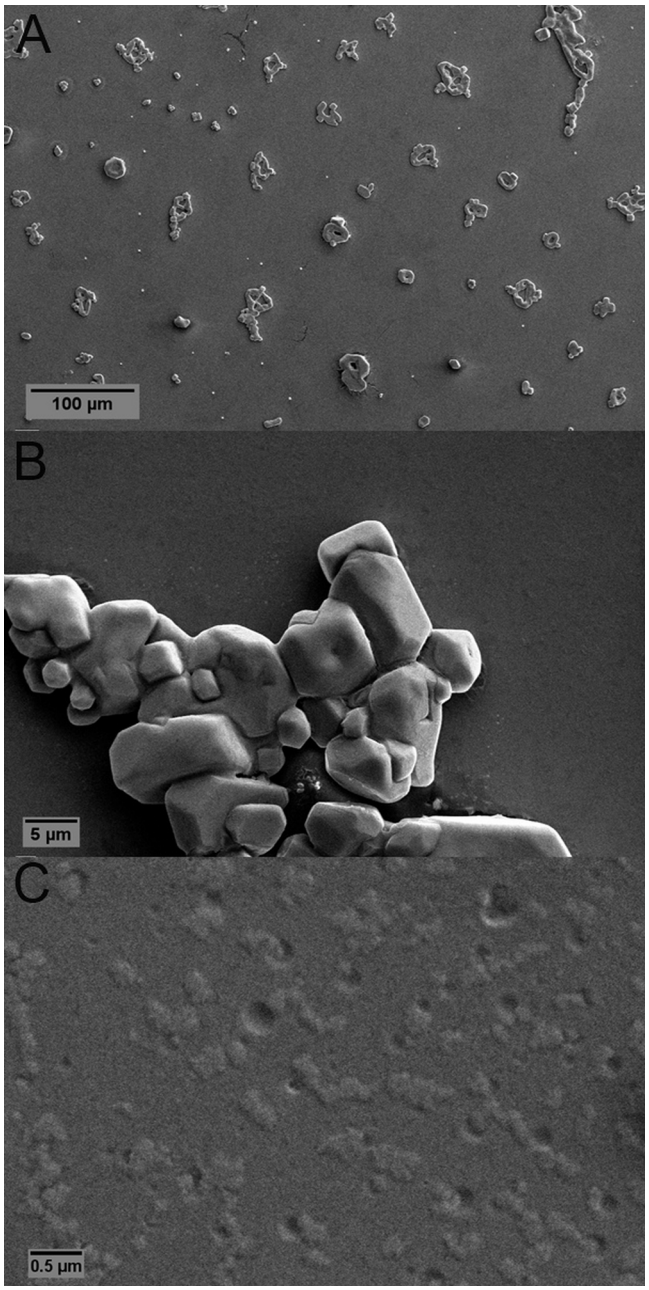

Fig. 3. SEM microphotographs of gliadin system at pH 7.0, 10 mM NaCl. (A) SEM image showing gliadin microstructures. (B) Zoom of image A, showing a cluster of microstructures. (C) Zoom of image B, showing the presence of nanostructures.

2.6.2. Transmission electron microscopy (TEM)

An electron microscope Philips CM 100 with a beam of 80 kV was used. Samples and deposited onto a grid cover with Formvar. Staining was performed with uranyl acetate following standard protocols.

All the Images were analyzed using Image J software.

2.7. Fractal analysis

Fractal analysis of the SEM images of gliadin at pH 3.0 was performed using Image J. The Box Counting algorithm was used to get the information about fractal properties. The topographic images were transformed to 8-bit binary format and the box values of 4, 8, 16, 32, 64 and 128 were overlaid in the image to obtain the fractal dimension (D_f) of the whole picture (see SI).

2.8. Circular dichroism

CD spectra of gliadin systems at pH 3.0 (0.065 mg/ml) and pH 7.0 (0.065 mg/ml) were recorded using a Jasco J-810CD spectrometer with a Peltier system as temperature controller. Usually, 3 scans were acquired in the range 190–250 nm at 20 °C. A scanning speed of 50 nm/min and 0.1 mm Quartz cuvettes were employed. Water solutions at pH 3.0 and 7.0 were measured under the same conditions and subtracted from the spectra. Smoothing and noise reduction was performed by a binomial method. Graphics were represented using the program OriginLab.

2.9. Nile red interaction

Gliadin systems were prepared as described in Sample Preparation section. All experiments were performed with a fresh solution of a 0.05 mM saturated Nile red (NR) in water using a Shimadzu RF spectrofluorophotometer at 20 °C. Excitation at 552 nm and 590 nm were performed and the emission spectra were collected in the range of 560–700 nm and 600–720 nm, respectively (the excitation and emission slits were of 3 and 5 nm respectively). The same procedure was carried out for only NR water solutions at pH 3.0 and 7.0, respectively. Titration experiments were carried out in order to obtain a global apparent binding constant. Increasing concentration of NR (0.05 mM) were added to 2 mL of gliadin solution and incubated for 10 min. Excitation at 552 nm at 25 °C was performed and emission spectra were acquired between 560 and 700 nm. Intensity of fluorescence was corrected by the inner filter effect, due to the ability of the dye to absorb the wavelength at which it is excited. This correction is performed by multiplying the fluorescence by the factor $10^{(A_{em}+A_{\lambda_{exc}}/2)}$. To apply this factor, absorption spectra of the NR at different concentrations at pH 3.0 and 7.0 at 10 mM NaCl were recorded using an optical path of 10 nm. Suitable calibration curves were realized to obtain the values A_{em} and $A_{\lambda_{exc}}$. Non-specific fluorescence was subtracted to the total intensity of fluorescence of gliadin system at the corresponding pH and NR concentration [25]. The obtained fluorescence spectra correspond to the specific fluorescence. Considering the shape of the titration curve of Nile red-protein, dissociation constant (K_d) was obtained by using Hill's regression provided by the software OriginLab.

2.10. Nile red release

Gliadin solution at pH 3.0 (0.168 mg/ml) was prepared as it was described before. A two mL of gliadin solution were taken and NR was added reaching a final concentration of 0.6 µM. After 10 min of incubation, two aliquots were separated and one of them was brought to 7.0. Both gliadin—NR mixtures were centrifuged at 21130*g* leading to a clear solution. Emission spectra of NR in both conditions were acquired and processed as describe above.

3. Result and discussion

3.1. Characterization of gliadin self-organized systems at pH 3.0 and 7.0 by SDS-PAGE, UV–vis spectroscopy, tryptophan steady state fluorescence spectroscopy and zeta potential

In order to mimic the stomach conditions, gliadin was dissolved under shaking in 0.001 M HCl, 10 mM NaCl, reaching pH 3.0. Considering that gliadin is not fully degraded in the stomach and reaches the duodenum [1], the pH of the solution was switched from 3.0 to 7.0. At pH 7.0, phase separation occurs observing the presence of macroscopic aggregates. Previously, Thewissen et al. [26] reported high solubility of wheat gliadin in aqueous media at extremely acidic and alkaline conditions, and poor solubility near neutral pH values, since the isoelectric point (I.P.) of gliadin is around 7.8

[27]. Both acidic and neutral solutions were centrifuged and further experiments were performed with the soluble fractions (see Section 2).

The identity of gliadin water soluble fractions, at pH 3.0 and 7.0 were determined by SDS-PAGE (Fig. 1(A). In both cases, the obtained bands showed molecular weight comparable with those previously reported for α and β isoforms [2,7]. The observed band intensity differences could be attributed to the decrease of soluble protein concentration after pH 7.0 was reached (see Section 2.1).

To obtain quickly global information about the system, UV/Vis spectroscopy was performed in the range between 250 and 400 nm (Fig. 1(B). Although both gliadin solutions were visible clear, it was possible to detect scatter at wavelengths >320 nm, which was more evident at pH 7.0, indicating the presence of aggregates (Fig. 1(B) [23]. Similar results have been reported previously for the formation of multimeric protein structures generated by fibrillation, polymerization, gelation, etc [28–30]. Given the characteristic of UV/Vis spectra of gliadin solutions between 350 and 400 nm, the percent aggregation index (A.I. [%]) was calculated taking into consideration the ratio A_{350}/A_{280} (see Section 2). Normally, when there is no aggregation, the A.I. is in the range of 0–2, in the presence of some aggregates is in the range of 2–5, and high aggregation shows values of A.I. higher than 5 [23,31]. At pH 3.0, the calculated A. I. was 3.8, meanwhile at pH 7.0 the A.I. was 17. 2.

The spontaneous assembly and induced aggregation of food proteins has been recently reviewed by Bouhallab et al. indicating that complex proteins are able to self-organize at physiological conditions [32,33].

Our results showed that gliadin in aqueous medium is able to self-organize differentially, while gliadin solution at pH 3.0 suggests moderate aggregation without phase separation, higher aggregation index was found after pH 7.0 was reached. Previously, it was reported similar results when gliadin nanoparticles were prepared from ethanolic solution by desolvation methods [7]. The strong aggregation at pH 7.0 could be explained by the well-known protein aggregation phenomenon at the isoelectric point. This process is attributed to the increment of attractive colloidal interactions over repulsive interactions near the isoelectric point, which is the force that leads to the formation of protein nanoparticles in general [34].

In addition, UV–vis spectroscopy provides very sensitive information about changes on the Tyr and Trp molecular environment related to folding or unfolding and aggregates formation. Although UV–vis spectroscopy is in the group of "low resolution" techniques, this method is especially useful in complex systems like food proteins obtaining structural information of the whole system [23,35]. In particular, gliadins are proteins with high content of Tyr amino acid, and only some isoforms of alpha gliadin posses a Trp in the primary structure [5,36]. First, to determinated the ratio Tyr: Trp in gliadin systems a methodology proposed by Bencze and Schmid was performed (see Section 2 and SI) [24]. This methodology offers an important advantage over chemical methods since it does not require sample hydrolysis, which often leads to partial decomposition of Tyr and Trp. In our studies a Tyr: Trp ratio of 2.26: 1 was obtained in gliadin solution at pH 3.0, while at pH 7.0 the ratio was 1.86: 1. These results are in agreement with previous reports describing similar ratios in gliadin samples, estimated by colorimetric and gravimetric methods [37–39]. Comparison of UV/Vis spectra at pH 3.0 and 7.0 (Fig. 1(B), showed that by changing the pH of the solution from 3.0 to 7.0, a decrease of gliadin concentration occurred as detected by the drop of the signal around 280 nm. The decrease of protein concentration was corroborated by Bradford's method and it explains the differences in the relative intensity of signals between pH 3.0 and 7.0 observed by SDS-PAGE (Fig. 1(A) (see Section 2).

Inspection of the UV/Vis spectra (Fig. 1(B) shows that the maximum wavelength absorption is around 282 nm, 2 nm red-shifted of the expected 280 nm wavelength maximum of free amino acids [35]. The second derivative spectrum enhances differences among spectra, resolves overlapping bands in qualitative analysis and most importantly, reduces the effect of interference from scattering (Fig. 1(C) [23]. In such spectra, the minimum observed around 280.0 nm corresponds to Tyr and Trp absorption, while the one around 290.0 nm belongs only to Trp. In general, wavelength shifts in the order of 0.1 nm are correlated with protein structural changes [23]. Considering Tyr and Trp absorption together, our gliadin system at pH 3.0 showed a minimum positioned at 281.5 nm, meanwhile the minimum was observed at 281.0 at pH 7.0. This redshift of 1.5 and 1.0 nm could be attributed to a less interaction of Tyr with the aqueous medium, being the amino acid buried into the structure. Thus, implies that gliadins are at some extend folded at both pHs. On the other hand, considering only Trp absorption, gliadin systems showed a minimum absorption at 288.7 nm at pH 3.0, while at pH 7.0 the minimum was observed at 288.5 nm. Here, the blueshift of 1.3–1.5 nm of the 290 nm band, at pH 3.0 and 7.0 respectively, suggest that Trp is exposed to water solvent in both cases, although not at the same extend.

Steady state fluorescence experiments were restricted to only Trp evaluation because it has a high quantum yield and its emission spectrum is sensitive to environment polarity [23,40]. Tyr fluorescence is not suitable because of its low sensibility to changes in the environment polarity, restricting its usefulness only to time resolved fluorescence experimemts [41]. To selectively excite Trp an excitation at 295 nm was used, and the emission spectra was recorded in the region between 307 and 350 nm, where the Trp emits depending on the environmental characteristics [42]. The emission spectrum of gliadin systems at both pHs showed a wide peak centered near 350 nm with a bandwidth of 60 nm (Fig. 1(D), suggesting the existence of different Trp species. To get a better resolution of the bands, and to characterize changes in the tertiary structure of both systems the second derivative spectrum at each pH is presented [42,43]. At pH 3.0, two minimums were detected at 334 and 345 nm, meanwhile at pH 7.0 both minimums were shifted to 332 and 346 nm, respectively. This demonstrates the existence of at least two types of Trp in both gliadin systems, one buried to the protein core (334–332 nm) and the other exposed to the solvent (345–346 nm) [42,44]. The first group may correspond to a Trp class I, in which this residue is located in a polar but rigid environment inside the protein, forming a 2:1 excimers with two neighboring polar groups (complex of two or more molecules that has low energy than the fluorophore). The second group may correspond to a Trp class II, where this residue is preferably in the surface of the protein, in contact with the solvent and other polar groups of the protein [45,46]. In both cases, Trps located in the surface may stabilize the system. This may occur by hydrogen bonding interactions with molecules of water and other polar groups favored by entropy as observed previously in protein viral capsids [47]. At pH 3.0, the relation between IF_{334}/IF_{345} is 0.98, showing that both Trps are uniformed distributed in the assembly. On the other side, at pH 7.0 the ratio IF_{332}/IF_{346} is 1.42, showing that more than half of the Trps are more buried and less exposed to the solvent upon pH increase.

In addition, upon increasing the pH from 3.0 to 7.0 gliadin Trp bands showed a blueshift of 2 nm for the first band from 334 to 332 nm, and a redshift of 1 nm of the second band from 345 to 346. These observations suggest that a change in the tertiary structure of gliadin system occurred due the change of pH, producing a more compact tertiary structure in the case of pH 7.0.

Our results show that at both pHs, gliadin is self-organized in water at 10 mM ionic strength. The spontaneous self-organization at pH 3.0 increases the apparent solubility due to the formation

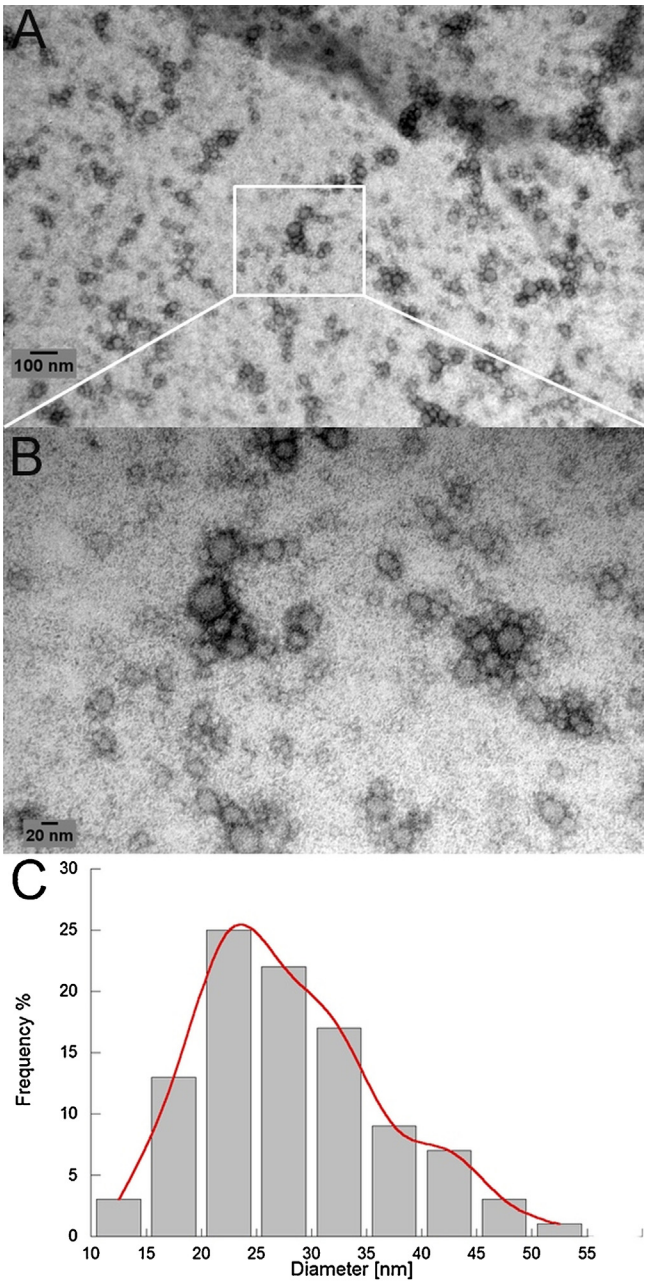

Fig. 4. TEM Microphotographs of gliadin system at pH 7.0, 10 mM NaCl. (A) TEM image showing gliadin structures and their association. (B) Zoom of image A, showing the different particles sizes. (C) Diameter distribution of the nanostructures observed in image A.

of finite sized aggregates, such as those formed in the micellization of amphiphilic molecules [48]. Switching the pH from 3.0 to 7.0 lead to a phase separation, however after centrifugation gliadin aggregates are disperse in the solution. Gliadin can be stabilized mainly by hydrophobic interactions due to its amino acid composition (proline, 14% and glutamine 40%), but also by salt bridges and hydrogen bonds. Taking into account that gliadin composition has a high content of glutamine, we hypothesized that hydrogen bonds with water can be responsible of gliadin colloidal stabilization [49].

The combination of short range attraction and long-range repulsion has been shown to result in the formation of equilibrium clusters during protein aggregation, in general. [50] In the simplest form of the DLVO theory, the attractive potential is represented by the van der Waals force between the particles in the medium, meanwhile the repulsive force between the particles arises due to the double layer overlap [51]. While the attractive potential remains nearly constant, the repulsive part of the potential is tuned over a large range by controlling the zeta potential through the pH, ionic strength, and temperature. The driving forces present in gliadin systems may be quantified by considering the tendency to spontaneously aggregate in solution, through electrokinetic measurements [52]. Zeta potential measurements show that at pH 3.0 the zeta potential was +13, 42 ± 1.55 mV, meanwhile at pH 7.0 was +4, 78 ± 0.48 mV. Both low zeta potential values are in the incipient instability regime, indicating that gliadin possesses an intrinsic instability [52,53]. However, particles are kinetically stabilized in solution at both pHs. The fact that gliadin carries only a slight charge, shows that a weak electrostatic repulsion would favors aggregates formation after the molecules are in contact [9]. Considering the moderate to high grade of aggregation observed at both pH, it is possible to affirm that although both solution are clear, both

systems are better described as self-organized solutions in water [54].

3.2. Morphology and secondary structure of gliadin self-organized solutions at pH 3.0 and 7.0 by electron microscopy and circular dichroism experiments

Gliadin ability to form spontaneously aggregates in aqueous media has been previously reported in acetic acid [6], mixtures ethanol/water [55] and more recently in distilled water [10]. In distilled water at very dilute concentration, it has been reported that gliadin is a rod-like shape monomer with a length of 11.3 nm and a width of 2.5 nm. The presence of oligomers has been also detected by SAXS and sedimentation experiments, however no direct visualization of the oligomers has been reported [10]. Previously, EM has provided adequate information about the morphology of oligomers and protein aggregates in vitro [16,56–58]. Here, EM of gliadin systems at pH 3.0 and 7.0 provided sufficient structural details for general morphological characterization of both systems. At pH 3.0, it was possible to detect two populations of nanostructures which average diameter of 17 ± 1.6 and 20.8 ± 2.0 nm. Interestingly, the structures are able to interact forming linear arrangements (Fig. 2(A) and (B). The size and morphology of the nanostructures are consistent with the formation of gliadin oligomers [52,53,59].

By SEM, it was detected that the nanostructures are able to further interact on glass surface forming fractal like patterns (Fig. 2(D). In general, the process of protein deposition and aggregation, which occurs when the solvent evaporates, eventually allows the precipitation of soluble species. This process results in complex architectures that are classified by physical properties, including fractal dimension (D_f), density and texture [52,59–61]. The fractal dimension was calculated by the counting box algorithm resulting in a D_f of 1.768 ± 0.034 [62]. This fractal dimension is consistent with scaling predictions [63], and explained by the presence of a polydisperse distribution of particles, providing additional nucleation sites for dendritic growth, increasing the D_f. The occurrence of fractal structures suggests that gliadin is able to further self-assembly process on glass by a fractal diffusion limited assembly mechanism (DLA) [17,52].

The relationship between low zeta potential and tendency for DLA has also been previously observed in colloidal systems and protein systems under low ionic strength [52,53]. We hypothesize that the presence of sufficiently weak or negligible energetic barrier because of the weaker surface charges between gliadin particles at pH 3.0, favors the DLA process on surface. DLVO theory supports this colloidal instability as a function of both van der Waals and electrostatic interactions between discrete particles undergoing Brownian motion [48]. A similar behavior has been recently reported for 33-mer gliadin peptide [17], and also for other complex systems like sericitin proteins which are the soluble fraction of silk [52].

Deposition of gliadin system at pH 7.0 on glass and SEM observation allowed the precipitation of amorphous microstructures and nanostructures (Fig. 3). The detection of the microstructures is in good agreement with the high aggregation index of 17.2 calculated by UV–vis spectroscopy.

An improved observation of nanostructures was obtained by TEM showing an average diameter of 27 ± 8.5 nm and the presence of nanoparticle clusters (Fig. 4). This results are in agreement with previous reports which have shown that the size and morphology of gliadin nanoparticles depend strongly on solvents and sample preparation [8].

The secondary structure evaluation was performed by circular dichroism experiments [64]. Previously, 33-mer gliadin self-assembly process occurred with secondary structure transition from extended structures like PPII to ordered ones like β sheets [16,17]. Moreover, in other proteins denaturation or unfolding is involved in the early stages of the aggregation process [18]. It is known that gliadins are composed mainly for random and alpha helix structures [65,66]. Because both samples are composed of mixtures of proteins the possibility to obtain a spectra in relation with the molar composition was not straightforward available; however, a qualitative comparison could be done. At pH 3.0 and 7.0 both systems showed the same CD patterns, showing that both are composed of random and α helices, ratio $\lambda_{208}/\lambda_{222}$, 1.85 and 1.87 at pH 3.0 and 7.0, respectively (see Fig. S4 in SI). This result is essentially the same as reported by Kasarda et al. for α gliadin at pH 3.0 and pH 5.0 in acetic acid and low ionic strength. Interestingly, Kasarda et al. did not observe important changes on secondary structure between randomly disperse gliadin and gliadin nanofibrils [65]. Other authors have reported that the CD spectrum of the gliadin mixture resembles those of isolated α gliadin [66]. Considering that gliadin soluble fraction at pH 7.0 is mainly composed of alpha gliadin, our results are reasonable. The small spectral differences could be due to slightly different protein concentration. Summarizing, our CD experiments showed that denaturation is not the responsible of formation of gliadin self-organized systems and that secondary structure is maintained at both pHs.

3.3. Nile red interactions with gliadin self-organized systems at pH 3.0 and 7.0

In general, protein self-assembled systems have been widely studied by extrinsic fluorescence in order to evaluate protein organization. [67] In particular, Nile red (NR) is a hydrophobic probe which senses changes in microenvironments [68]. Previously, NR was used to monitor changes in the hydrophobicity surface of proteins such as cytochrome P450 3A4 [69] but also in different protein aggregates [70] such as those of β-galactosidase [71] amyloid fibrils [72] and also to elucidate the intermediates in the self-assembly of tubulin [73]. In a low polar environment, NR fluorescence is increased and a blueshift of wavelength maximum emission is detected [68,74]. Moreover, the large blueshift observed (108 nm from water to hexane) [75] makes possible to excite probe molecules selectively in different microenvironments. These characteristics of NR lead to an excitation dependent-emission maximum (λ_{max}) when different microdomains in the aggregate are present [68,74,76]. This property is of a great advantage in order to determinate binding of NR in highly aggregated solutions, like this of gliadin at pH 7.0. When NR is excited at 552 or 590 nm, the emission spectra are only derived from the polar interface, thus a dependent emission maximum is expected if NR binds to gliadin systems [74]. The λ_{max} of emission, were accurately determined by second derivative methodology [76].

Initially, NR in water at pH 3.0 or 7.0 were excited at 552 and 590 nm, observing an emission peak at 640 nm and no dependence of the emission maximum (Fig. 5 and Fig. 6). When gliadin-NR system at pH 3.0 was excited at 552 nm (Fig. 4), the maximum emission was blue shifted to 608 nm, however the band at 640 nm persisted. Excitation at 590 nm showed a blueshift of the maximum to around 620 nm, however the band was really broad suggesting the presence of different binding sites. The maximum wavelength blueshift is consistent with the presence of gliadin self-organized aggregates which possess hydrophobic binding sites for the NR binding. Owing to the large polarity-dependent absorbance shift of NR, the probe which resides more toward the core of the aggregates will be excited at lower wavelength and emits at a lower wavelength [74]. By contrast, the probe residing more toward the outside of the aggregate (facing water solvent) will be preferentially excited and emits at higher wavelength. The new blueshifted value close to 608 nm was previously reported in the case of inverted micelles of amphiphiles [70,76] and of β-galactosidase aggregates [71].

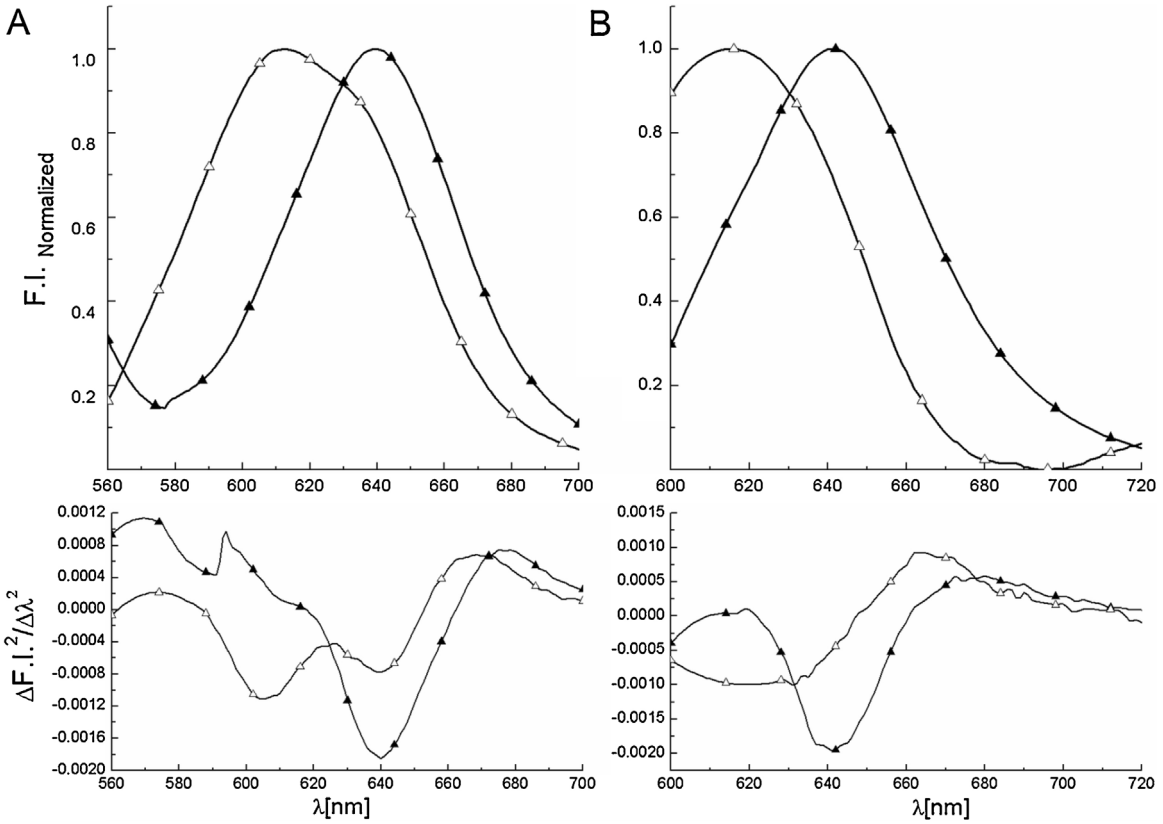

Fig. 5. Normalized fluorescence emission spectrum of gliadin-NR system at pH 3.0, NaCl 10 mM (Δ), and only NR in water at pH 3.0 (▲) under the same experimental condition. Excitation wavelength: (A) 552 nm and (B) 590 nm. The corresponding second derivative spectra were below each graphic.

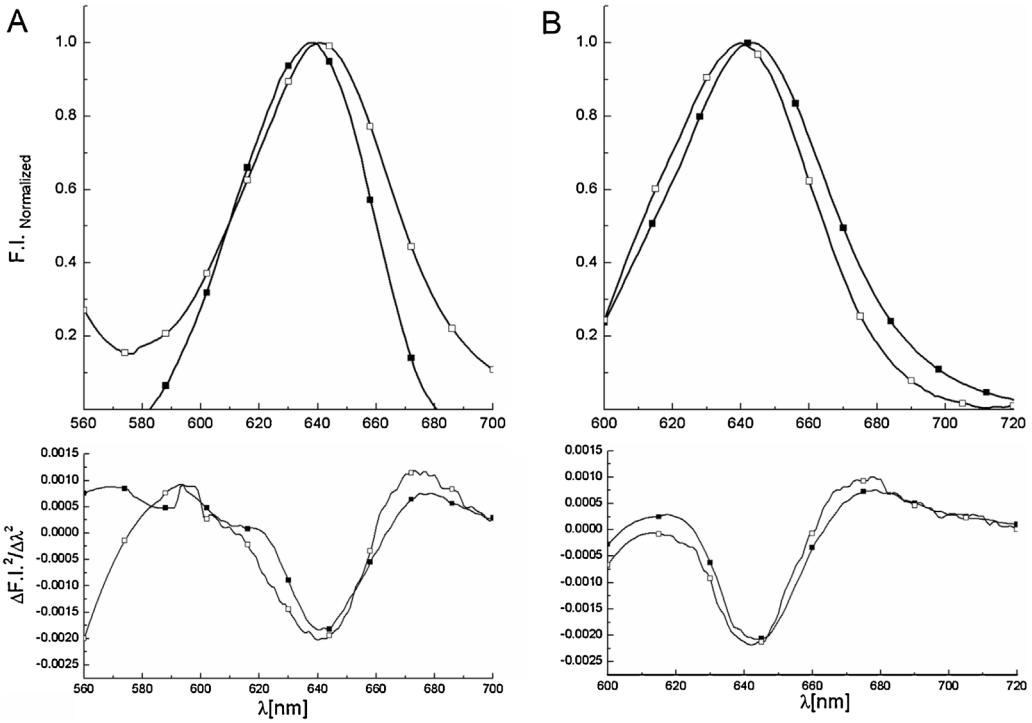

Fig. 6. Normalized Fluorescence Emission spectrum of gliadin-NR system at pH 7.0, NaCl 10 mM (Δ), and only NR in water at pH 7.0 (▲) under the same experimental condition. Excitation wavelength: (A) 552 nm and B) 590 nm. The corresponding second derivative spectra were below each graphic.

On the other hand, at pH 7.0 no excitation dependent emission was detected as shown in Fig. 6.

Our findings show that the nature of the surfaces of gliadin self-organized is quite different. At pH 3.0, it was evidenced the presence of accessible hydrophobic binding sites, whereas at pH 7.0 the NR

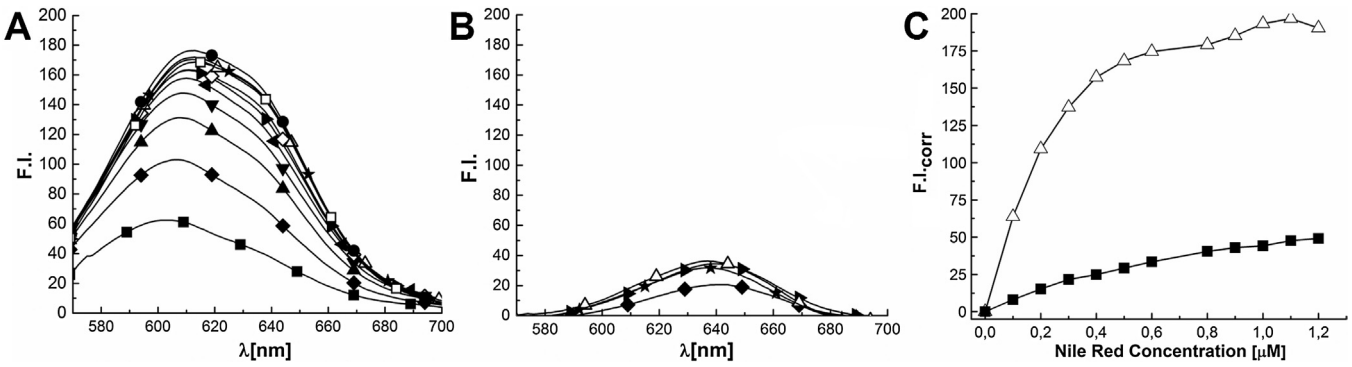

Fig. 7. Titration of gliadin systems with Nile red. Emission spectra of the gliadin: NR mixtures at (A) pH 3.0, NR final concentration: 0.1 μM (■), 0.2 μM (♦), 0.3 μM (▲),0.4 μM (▼), 0.5 μM (◄),0.6 μM (►),0.8 μM (◊), 0.9 μM (Δ), 1.0 μM (⋆), 1.1 μM (l), 1.2 μM (□) and (B) at pH 7.0, NR final concentration: 0.2 μM (♦),0.6 μM (►),0.9 μM (Δ), 1.1 μM (⋆). C) Binding curves at pH 3.0 at: 608 nm: specific binding (Δ) and free ligand (■). For all spectra NR contribution in water at pH 3.0 or 7.0 were subtracted.

probe was not able to interact with gliadin, showing that the surface of the aggregates at pH 7.0 is highly polar and/or hydrophobic patches are not accessible.

To quantify the NR binding, a titration was carried out increasing probe concentration and using an excitation wavelength of 552 nm (Fig. 7).

NR titration at pH 3.0 showed that the λ_{max} of emission was red shifted from 599 to 608 nm upon increasing NR concentration, and the shoulder at 640 nm was more evident at high NR concentration. The global apparent dissociation constant was determined according to Hill adjustment at 608 showing a K_d value of 0.180 ± 0.080 μM. The band of λ_{max} around 608 nm is typically observed when NR molecules are incorporated in hydrophobic cores, in protein surfaces or aggregates such as core-shell particles, micelles or vesicles [68–75]. Probably, the band arounf 608 nm correspond to NR in the interior of the aggregates and the second band at 640 nm to those NR molecules more exposed to the solvent. The sequential red shift of the band shows that different hydrophobic sites are accessible to NR and can be attributed to a progressive filling of the binding sites, depending on binding affinity. In addition, the appearance of a shoulder at higher wavelength was previously observed in cytochrome P450 3A4 [69] and tubulin aggregates [73]. Based on our findings, we hypothethised that gliadin at pH 3 is able to form micelle type aggregates under the experimental conditions tested.

On the other hand, although the intensity of the emission of Nile red at 640 nm was slightly increased at pH 7.0, no binding constant could be calculated. And more importantly, no shift of the maximum emission band was observed. This confirms that the surface area of gliadin aggregates at pH 7.0 has a polar nature or/and that the hydrophobic sites are not accessible to NR. Incubation of NR-gliadin mixture for at for at least 30 min did not lead to changes in NR emission spectrum. Considering the existence of colloidal nanoparticles at pH 7.0, we hypothesized that the surface of gliadin particles interacts strongly with water, probably with glutamine amino acid, thus lowering the interaction with NR or a quenching of NR fluorescence intensity (due to H-bonding) can be expected [74]. The presence of a shell of tightly bound water molecules can prevent gliadin particles from further aggregation and precipitation when they collide, reinforcing the idea of colloidal stabilization in water.

Finally, the *in situ* NR binding differences of gliadin self-organized structures at both pHs were tested by switching the pH from 3.0 to 7.0 (Fig. 8). Measurements of intensity of fluorescence of NR have previously shown changes in supramolecular organization depending on external stimulus [76,77].

As expected, at pH 3.0 gliadin self-organized structures showed fluorescence intensity at 608 nm, while switching to 7.0 a decrease

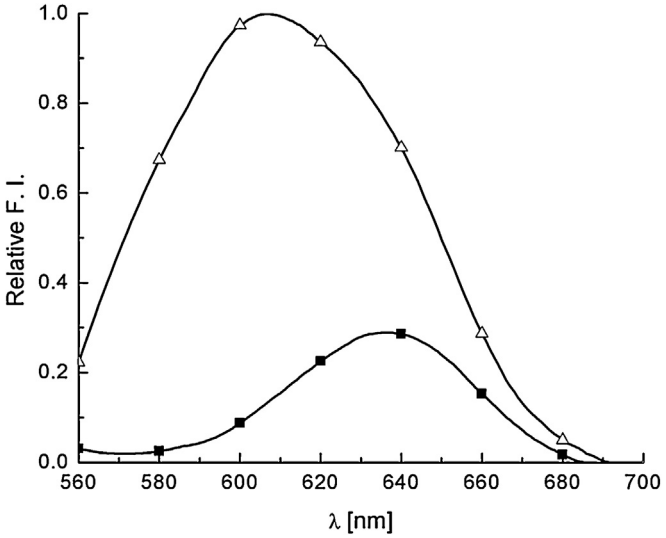

Fig. 8. Nile red spectrum of gliadin system at pH 3.0 (■) and after switch of pH to 7.0 (□). NR contribution in water at pH 3.0 or 7.0 was subtracted.

of fluorescence intensity and a red-shift to 640 nm was detected. This behavior suggests a change in gliadin self-organization *in situ* modulated by the pH, from micelle type aggregates to colloidal nanoparticles. Scheme 1.

4. Conclusion

The spontaneous self-organization of gliadin in water at pH 3.0 and 7.0 under low ionic strength was reported. Our findings support the hypothesis of spontaneous micellization of α and β gliadin isoforms at pH 3.0, although in the incipient instability regime ($\zeta = +13, 42 \pm 1.55$ mV), the repulsive component exhibits a barrier, thus nanostructures are kinetically stabilized. On TEM grid, most of the particles are separated, but on glass surface they are able to further interact by a fractal DLA mechanism (see SEM, Fig. 2). As mentioned, similar behavior has been recently reported for 33-mer gliadin peptide [16,17] and other protein like sericitin [52] and sillicatein [78] under low ionic strength. Later on, upon increase the pH to 7.0, gliadin nanostructures repulsion decrease due to the proximity to the isoelectric point, and the electrostatic repulsive force between particles was negligible ($\zeta = +4, 78 \pm 0.48$ mV). Thus it is likely that particles adhere once they encounter each other in the solution, leading to the observed decrease of solubility. After centrifugation, colloidal gliadin nanoparticles are stabilized probably because H-bond with water molecules. Deposition of gliadin

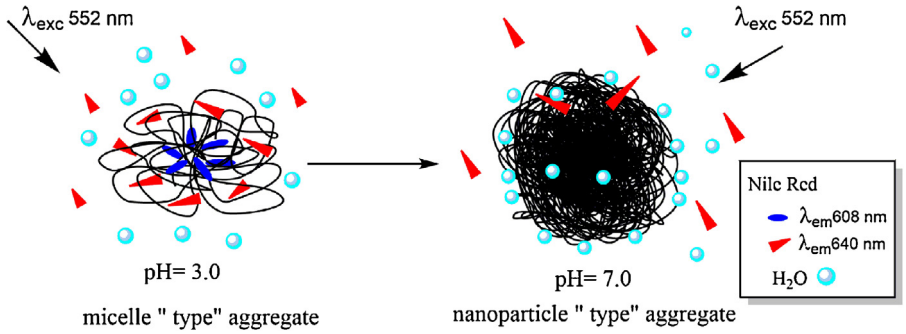

Scheme 1. Cartoon representing gliadin micelle type aggregates (pH 3.0) and nanoparticles (pH 7.0) in water system. Triangles represent Nile Red molecule emitting at λ_{max} 608 nm (blue) and λ_{max} 640 nm (red) when excited at 552 nm. Interaction depends on accessibility to hydrophobic cores and the presence of water strongly bound to the aggregates. (For interpretation of the references to colour in this figure legend, the reader is referred to the web version of this article).

at pH 7.0 on glass and SEM observation showed the presence of amorphous aggregates in the micrometer range and nanoparticles. On TEM grid, the nanostructures formed clusters. Recently, gliadin nanoparticles formation were reported in distilled water (probably at pH 6–7) [10].

The supramolecular transition from micelles to nanoparticles modulated by pH were also reported for casein protein but casein transition occurred upon decreasing pH [79].

Previously, it has been reported that gliadin is not completely degraded by pepsin (pH 2–3) and trypsin (pH 7.0) *in vitro* and *in vivo* (in murine models) [1], although 54 cutting sites for both enzymes are theoretically possible [80]. The occurrence of colloidal nanostructures can explain the up to now unexpected proteolytical resistance, and thus the hypothesis of incapability of digestive enzymes to access to the degradation sites of gliadin is reasonable. Moreover, considering the reported innate immunological response triggered by gliadin, mainly at pH 7.0 [12,14,21], again the hypothesis of colloidal nanoparticles of gliadin as potential real triggers instead of randomly disperse gliadin can explain the reported immune and tissue stress behavior. Our research efforts are directed to test this hypothesis *in vitro* and *in vivo*.

In addition, because of the importance and variability of pH in the GI [19], our research effort will be focused toward a systematic evaluation of gliadin under different conditions by 3D correlation light scattering and small angle X diffraction. Meanwhile, our findings of gliadin spontaneous self-organization at relevant physiological pH and concentration might be a first step toward the understanding of gliadin *in vitro* and *in vivo* behavior.

Acknowledgments

This work was supported by CONICET (National Scientific and Technical Research Council), and UNS (Universidad Nacional del Sur) Argentinian Research grants, and partially by Alexander von Humboldt Foundation. M. G. H and T.V. V. are also grateful for their CONICET fellowships. V. I. D. thanks Prof. N. Sewald from Fakultät Chemie, Universität Bielefeld for his support to start this research project.

Appendix A. Supplementary data

Supplementary data associated with this article can be found, in the online version, at http://dx.doi.org/10.1016/j.colsurfb.2016.02.019.

References

[1] L. Shan, O. Molberg, I. Parrot, F. Hausch, F. Filiz, G.M. Gray, L.M. Sollid, C. Khosla, Structural basis for gluten intolerance in celiac sprue, Science 297 (2002) 2275–2279.
[2] K.A. Caldwell, A comparative study of disulphide-Bonding and molecular weights of purified fractions from secalin, gliadin, and hordein, J. Exp. Bot. 34 (1983) 1411–1420.
[3] G.L. Mills, Some observations on the electrophoresis of gliadin, Biochim. Biophys. Acta 14 (1954) 274–281.
[4] J.E. Bernardin, D.D. Kasarda, D.K. Mecham, Preparation and characterization of alpha-gliadin, J. Biol. Chem. 242 (1967) 445–450.
[5] T. Terce-Laforgue, L. Charbonnier, J. Mosse, Isolation and characterization of beta-gliadin fractions, Biochim. Biophys. Acta 625 (1980) 118–126.
[6] D.D. Kasarda, J.E. Bernardin, R.S. Thomas, Reversible aggregation of alpha-gliadin to fibrils, Science 155 (1967) 203–205.
[7] I. Ezpeleta, J.M. Irache, S. Stainmesse, C. Chabenat, J. Gueguen, Y. Popineau, A.-M. Orecchioni, Gliadin nanoparticles for the controlled release of all-trans-retinoic acid, Int. J. Pharm. 131 (1996) 191–200.
[8] I.J. Duclairoir C, Nakache E, Orecchioni A-M, Chabenat C, Popineau Y, Gliadin nanoparticles: formation, all-trans −retinoic acid entrapment and release, size optimization, Polymer International, 48 (1999) 327–333.
[9] I.J. Joye, V.A. Nelis, D.J. McClements, Gliadin-based nanoparticles: fabrication and stability of food-grade colloidal delivery systems, Food Hydrocolloids 44 (2015) 86–93.
[10] N. Sato, A. Matsumiya, Y. Higashino, S. Funaki, Y. Kitao, Y. Oba, R. Inoue, F. Arisaka, M. Sugiyama, R. Urade, Molecular assembly of wheat gliadins into nanostructures: a small-angle X-ray scattering study of gliadins in distilled water over a wide concentration range, J. Agric. Food Chem. 63 (2015) 8715–8721.
[11] V. De Re, L. Caggiari, M. Tabuso, R. Cannizzaro, The versatile role of gliadin peptides in celiac disease, Clin. Biochem. 46 (2013) 552–560.
[12] S. Drago, R. El Asmar, M. Di Pierro, M. Grazia Clemente, A. Tripathi, A. Sapone, M. Thakar, G. Iacono, A. Carroccio, C. D'Agate, T. Not, L. Zampini, C. Catassi, A. Fasano, Gliadin, zonulin and gut permeability: effects on celiac and non-celiac intestinal mucosa and intestinal cell lines, Scand. J. Gastroenterol. 41 (2006) 408–419.
[13] A. Sapone, J.C. Bai, C. Ciacci, J. Dolinsek, P.H. Green, M. Hadjivassiliou, K. Kaukinen, K. Rostami, D.S. Sanders, M. Schumann, R. Ullrich, D. Villalta, U. Volta, C. Catassi, A. Fasano, Spectrum of gluten-related disorders: consensus on new nomenclature and classification, BMC Med. 10 (2012) 13.
[14] A. Fasano, A. Sapone, V. Zevallos, D. Schuppan, Nonceliac gluten sensitivity, Gastroenterology 148 (2015) 1195–1204.
[15] K.E. Lundin, L.M. Sollid, Advances in coeliac disease, Curr. Opin. Gastroenterol. 30 (2014) 154–162.
[16] M.G. Herrera, F. Zamarreno, M. Costabel, H. Ritacco, A. Hutten, N. Sewald, V.I. Dodero, Circular dichroism and electron microscopy studies in vitro of 33-mer gliadin peptide revealed secondary structure transition and supramolecular organization, Biopolymers 101 (2014) 96–106.
[17] M.G. Herrera, L.A. Benedini, C. Lonez, P.L. Schilardi, T. Hellweg, J.M. Ruysschaert, V.I. Dodero, Self-assembly of 33-mer gliadin peptide oligomers, Soft Matter 11 (2015) 8648–8660.
[18] P. Taboada, S. Barbosa, J. Juárez, M.-A. Meda, V. Mosquera, Amyloid-like Fibrils: Origin, Structure, Properties, and Potential Technological Applications, Proteins in Solution and at Interfaces, john wiley & sons, New Jersey, 2013 (Chapter 12.).
[19] S. Bellmann, D. Carlander, A. Fasano, D. Momcilovic, J.A. Scimeca, W.J. Waldman, L. Gombau, L. Tsytsikova, R. Canady, D.I. Pereira, D.E. Lefebvre, Mammalian gastrointestinal tract parameters modulating the integrity, surface properties, and absorption of food-relevant nanomaterials, Wiley interdisciplinary reviews, Nanomed. Nanobiotechnol. 7 (2015) 609–622.
[20] J. Visser, J. Rozing, A. Sapone, K. Lammers, A. Fasano, Tight junctions, intestinal permeability, and autoimmunity: celiac disease and type 1 diabetes paradigms, Ann. N. Y. Acad. Sci. 1165 (2009) 195–205.
[21] M. Sellitto, G. Bai, G. Serena, W.F. Fricke, C. Sturgeon, P. Gajer, J.R. White, S.S. Koenig, J. Sakamoto, D. Boothe, R. Gicquelais, D. Kryszak, E. Puppa, C. Catassi, J. Ravel, A. Fasano, Proof of concept of microbiome-metabolome analysis and delayed gluten exposure on celiac disease autoimmunity in genetically at-risk infants, PLoS One 7 (2012) e33387.

[22] M. Okuda, Y. Uemura, N. Tatsumi, Quality control material for plasma fibrinogen test produced from purified human fibrinogen, J. Autom. Methods Manag. Chem. 25 (2003) 79–85.
[23] R. Esfandiary, C.R. Middaugh, Ultraviolet absorption spectroscopy, in: Analysis of Aggregates and Particles in Protein Pharmaceuticals, John Wiley & Sons, New Jersey, 2012 (Chapter 8).
[24] W.L. Bencze, K. Schmid, Determination of tyrosine and tryptophan in proteins, Anal. Chem. 29 (1957) 1193–1196.
[25] H.J. Motulsky, R.R. Neubig, Analyzing Binding Data, Current Protocols in Neuroscience, John Wiley & Sons, 2001, Unit 7.5.
[26] B.G. Thewissen, I. Celus, K. Brijs, J.A. Delcour, Foaming properties of wheat gliadin, J. Agric. Food Chem. 59 (2011) 1370–1375.
[27] Y.V. Wu, R.J. Dimler, Hydrogen ion equilibria of wheat glutenin and gliadin, Arch. Biochem. Biophys. 103 (1963) 310–318.
[28] G. Jiang, S.B. Joshi, L.J. Peek, D.T. Brandau, J. Huang, M.S. Ferriter, W.D. Woodley, B.M. Ford, K.D. Mar, J.A. Mikszta, C.R. Hwang, R. Ulrich, N.G. Harvey, C.R. Middaugh, V.J. Sullivan, Anthrax vaccine powder formulations for nasal mucosal delivery, J. Pharm. Sci. 95 (2006) 80–96.
[29] G. Marx, Divalent cations induce protofibril gelation, Am. J. Hematol. 27 (1988) 104–109.
[30] P.D. Yurchenco, E.C. Tsilibary, A.S. Charonis, H. Furthmayr, Laminin polymerization in vitro. Evidence for a two-step assembly with domain specificity, J. Biol. Chem. 260 (1985) 7636–7644.
[31] W. Wang, Y.J. Wang, D.Q. Wang, Dual effects of Tween 80 on protein stability, Int. J. Pharm. 347 (2008) 31–38.
[32] S. Bouhallab, T. Croguennec, Spontaneous assembly and induced aggregation of food proteins, in: M. Müller (Ed.), Polyelectrolyte Complexes in the Dispersed and Solid State II, Springer, Berlin Heidelberg, 2014, pp. 67–101.
[33] M. Boulet, M. Britten, F. Lamarche, Aggregation of some food proteins in aqueous dispersions: effects of concentration, pH and ionic strength, Food Hydrocolloids 14 (2000) 135–144.
[34] K. Langer, S. Balthasar, V. Vogel, N. Dinauer, H. von Briesen, D. Schubert, Optimization of the preparation process for human serum albumin (HSA) nanoparticles, Int. J. Pharm. 257 (2003) 169–180.
[35] V.I. Dodero, P.V. Messina, Analyzing the solution state of protein structure, interactions, and ligands by spectroscopic methods, in: Proteins in Solution and at Interfaces, John Wiley & Sons, New Jersey, 2013 (Chapter 4).
[36] D.D. Kasarda, T.W. Okita, J.E. Bernardin, P.A. Baecker, C.C. Nimmo, E.J. Lew, M.D. Dietler, F.C. Greene, Nucleic acid (cDNA) and amino acid sequences of alpha-type gliadins from wheat (*Triticum aestivum*), Proc. Natl. Acad. Sci. U. S. A. 81 (1984) 4712–4716.
[37] J.M. Looney, The colorimetric estimation of tyrosine, tryptophane, and cysteine in proteins. II, J. Biol. Chem. 69 (1926) 519–538.
[38] E.J. Cohn, J.L. Hendry, A.M. Prentiss, Studies in the physical chemistry of the proteins: tD:-V. the molecular weights of the proteins. part 1. The minimal molecular weights of certain proteins, J. Biol. Chem. 63 (1925) 721–766.
[39] J.A. Ewart, Amino acid analyses of glutenins and gliadins, J. Sci. Food Agric. 18 (1967) 111–116.
[40] J. Lakowicz Principles, of Fluorescence Spectroscopy, 2007.
[41] M. Amaro, D.J. Birch, O.J. Rolinski, Beta-amyloid oligomerisation monitored by intrinsic tyrosine fluorescence, Phys. Chem. Chem. Phys. 13 (2011) 6434–6441.
[42] V. Kumar, V.K. Sharma, D.S. Kalonia, Second derivative tryptophan fluorescence spectroscopy as a tool to characterize partially unfolded intermediates of proteins, Int. J. Pharm. 294 (2005) 193–199.
[43] S. Muzammil, Y. Kumar, S. Tayyab, Molten globule-like state of human serum albumin at low pH, Eur. J. Biochem. 266 (1999) 26–32.
[44] A. Mozo-Villarias, Second derivative fluorescence spectroscopy of tryptophan in proteins, J. Biochem. Biophys. Methods 50 (2002).
[45] A.S. Ladokhin, Fluorescence Spectroscopy in Peptide and Protein Analysis, Encyclopedia of Analytical Chemistry, John Wiley & Sons, 2006.
[46] E.A. Burstein, N.S. Vedenkina, M.N. Ivkova, Fluorescence and the location of tryptophan residues in protein molecules, Photochem. Photobiol. 18 (1973) 263–279.
[47] A.T. Da Poian, J.E. Johnson, J.L. Silva, Protein-RNA interactions and virus stability as probed by the dynamics of tryptophan side chains, J. Biol. Chem. 277 (2002) 47596–47602.
[48] J.N. Israelachvili, Thermodynamic principles of self-Assembly, in: J.N. Israelachvili (Ed.), Intermolecular and Surface Forces (Third Edition), Academic Press, San Diego, 2016 (Chapter 19).
[49] A.O. Elzoghby, W.M. Samy, N.A. Elgindy, Protein-based nanocarriers as promising drug and gene delivery systems, J. Control. Release 161 (2012) 38–49.
[50] A. Stradner, H. Sedgwick, F. Cardinaux, W.C. Poon, S.U. Egelhaaf, P. Schurtenberger, Equilibrium cluster formation in concentrated protein solutions and colloids, Nature 432 (2004) 492–495.
[51] D. Leckband, J. Israelachvili, Intermolecular forces in biology, Q. Rev. Biophys. 34 (2001) 105–267.
[52] N.E. Kurland, J. Kundu, S. Pal, S.C. Kundu, V.K. Yadavalli, Self-assembly mechanisms of silk protein nanostructures on two-dimensional surfaces, Soft Matter 8 (2012) 4952–4959.
[53] B. Viswanath, S. Patra, N. Munichandraiah, N. Ravishankar, Nanoporous Pt with high surface area by reaction-limited aggregation of nanoparticles, Langmuir 25 (2009) 3115–3121.
[54] K. Shinoda, A new concept ideal organized solution: comparison of random mixing solutions and ideal organized solution, Langmuir 7 (1991) 2877–2880.
[55] N.H. Thomson, M.J. Miles, Y. Popineau, J. Harries, P. Shewry, A.S. Tatham, Small angle X-ray scattering of wheat seed-storage proteins: alpha-, gamma- and omega-gliadins and the high molecular weight (HMW) subunits of glutenin, Biochim. Biophys. Acta 1430 (1999) 359–366.
[56] J.J. Miranda, P. De Wulf, P.K. Sorger, S.C. Harrison, The yeast DASH complex forms closed rings on microtubules, Nat. Struct. Mol. Biol. 12 (2005) 138–143.
[57] G.P. Lopez, H.A. Biebuyck, R. Harter, A. Kumar, G.M. Whitesides, Fabrication and imaging of two-dimensional patterns of proteins adsorbed on self-assembled monolayers by scanning electron microscopy, J. Amer. Chem. Soc. 115 (1993) 10774–10781.
[58] V.L. Anderson, W.W. Webb, Transmission electron microscopy characterization of fluorescently labelled amyloid beta 1–40 and alpha-synuclein aggregates, BMC Biotechnol. 11 (2011) 125.
[59] G. Jean-Francois, Physics and Fractal Structures 1996.
[60] M. Tokuyama, K. Kawasaki, Fractal dimensions for diffusion-limited aggregation, Phys. Lett. A 100 (1984) 337–340.
[61] J. Choi, D. Crowdy, M.Z. Bazant, Diffusion-limited aggregation on curved surfaces, EPL (Europhys. Lett.) 91 (2010) 46005.
[62] V.K. Yadavalli, D.V. Svintradze, R.M. Pidaparti, Nanoscale measurements of the assembly of collagen to fibrils, Int. J. Biol. Macromol. 46 (2010) 458–464.
[63] P. Ossadnik, C.-H. Lam, L.M. Sander, Nonuniversal diffusion-limited aggregation and exact fractal dimensions, Phys. Rev. E 49 (1994) R1788–R1791.
[64] V.I. Dodero, Z.B. Quirolo, M.A. Sequeira, Biomolecular studies by circular dichroism, Front. Biosci. 16 (2011) 61–73.
[65] D.D. Kasarda, J.E. Bernardin, W. Gaffield, Circular dichroism and optical rotatory dispersion of alpha-gliadin, Biochemistry 7 (1968) 3950–3957.
[66] Y.V. Wu, J.E. Cluskey, Optical rotatory dispersion studies on wheat gluten proteins: gluten, glutenin, and gliadin in urea and hydrochloric acid solutions, Arch. Biochem. Biophys. 112 (1965) 32–36.
[67] L.A. Munishkina, A.L. Fink, Fluorescence as a method to reveal structures and membrane-interactions of amyloidogenic proteins, Biochim. Biophys. Acta 1768 (2007) 1862–1885.
[68] P. Greenspan, E.P. Mayer, S.D. Fowler, Nile red: a selective fluorescent stain for intracellular lipid droplets, J. Cell Biol. 100 (1985) 965–973.
[69] A. Nath, C. Fernandez, J.N. Lampe, W.M. Atkins, Spectral resolution of a second binding site for Nile Red on cytochrome P4503A4, Arch. Biochem. Biophys. 474 (2008) 198–204.
[70] R.A. Poole, A. Hawe, W. Jiskoot, K. Braeckmans, Fluorescence Spectroscopy to Characterize Protein Aggregates and Particles, Analysis of Aggregates and Particles in Protein Pharmaceuticals, John Wiley & Sons, 2016 (Chapter 9).
[71] M. Sutter, S. Oliveira, N.N. Sanders, B. Lucas, A. van Hoek, M.A. Hink, A.J. Visser, S.C. De Smedt, W.E. Hennink, W. Jiskoot, Sensitive spectroscopic detection of large and denatured protein aggregates in solution by use of the fluorescent dye Nile red, J. Fluoresc. 17 (2007) 181–192.
[72] R. Mishra, D. Sjolander, P. Hammarstrom, Spectroscopic characterization of diverse amyloid fibrils in vitro by the fluorescent dye Nile red, Mol. Biosyst. 7 (2011) 1232–1240.
[73] D.L. Sackett, J.R. Knutson, J. Wolff, Hydrophobic surfaces of tubulin probed by time-resolved and steady-state fluorescence of nile red, J. Biol. Chem. 265 (1990) 14899–14906.
[74] M.C.A. Stuart, J.C. van de Pas, J.B.F.N. Engberts, The use of Nile red to monitor the aggregation behavior in ternary surfactant–water–organic solvent systems, J. Phys. Org. Chem. 18 (2005) 929–934.
[75] J.F. Deye, T.A. Berger, A.G. Anderson, Nile Red as a solvatochromic dye for measuring solvent strength in normal liquids and mixtures of normal liquids with supercritical and near critical fluids, Anal. Chem. 62 (1990) 615–622.
[76] C. Lin, J. Zhao, R. Jiang, Nile red probing for the micelle-to-vesicle transition of AOT in aqueous solution, Chem. Phys. Lett. 464 (2008) 77–81.
[77] I.N. Kurniasih, H. Liang, S. Kumar, A. Mohr, S.K. Sharma, J.P. Rabe, R. Haag, A bifunctional nanocarrier based on amphiphilic hyperbranched polyglycerol derivatives, J. Mater. Chem. B 1 (2013) 3569–3577.
[78] M.M. Murr, D.E. Morse, Fractal intermediates in the self-assembly of silicatein filaments, Proc. Natl. Acad. Sci. U.S.A. 102 (2005) 11657–11662.
[79] C. Moitzi, A. Menzel, P. Schurtenberger, A. Stradner, The pH induced sol–gel transition in skim milk revisited. A detailed study using time-resolved light and X-ray scattering experiments, Langmuir 27 (2011) 2195–2203.
[80] E. Gasteiger, A. Gattiker, C. Hoogland, I. Ivanyi, R.D. Appel, A. Bairoch, ExPASy: the proteomics server for in-depth protein knowledge and analysis, Nucleic Acids Res. 31 (2003) 3784–3788.